Geochemistry, Geophysics, Geosystems

RESEARCH ARTICLE
10.1029/2020GC009300

A Recent Tear in Subducting Plate Explains Seismicity and Upper Mantle Structure of Southern Costa Rica

J. Bourke[1], V. Levin[1], L. Linkimer[2], and I. Arroyo[2]

[1]Department of Earth and Planetary Sciences, Rutgers University, Piscataway, NJ, USA, [2]Escuela Centroamericana de Geología y Red Sismológica Nacional (RSN: UCR-ICE) Apdo, San Pedro, San José, Costa Rica

Key Points:

- This study constrains the seismic properties beneath the Cordillera de Talamanca of southern Costa Rica
- We observe an anomalous impedance increase with depth in the upper mantle beneath the upper plate Moho that is also separated from the subducting Cocos plate
- We propose that this feature is a piece of detached lithosphere caused by the migration of the Panama Triple Junction through Costa Rica

Supporting Information:

- Supporting Information S1

Correspondence to:

J. Bourke,
jrb370@eps.rutgers.edu

Citation:

Bourke, J., Levin, V., Linkimer, L., & Arroyo, I. (2020). A recent tear in subducting plate explains seismicity and upper mantle structure of southern Costa Rica. *Geochemistry, Geophysics, Geosystems*, *21*, e2020GC009384. https://doi.org/10.1029/2020GC009300

Received 15 JUL 2020
Accepted 9 NOV 2020

Abstract Past studies of southern Costa Rica have generated a multitude of tectonic scenarios to account for different data sets. Flat slabs, detached slabs, and slab windows have been proposed to address the uplift of the Cordillera de Talamanca (CT), cessation of volcanism, and absence of deep seismicity beneath southern Costa Rica. In this study, we investigate the crust and the upper mantle along the southwest flank of the CT using the receiver function methodology. We observe two regional positive P-to-S converted pulses at delay times of ~2–4 s and ~5–8 s. The first likely represents a gradational crust-mantle boundary of the upper plate. The second represents a similar impedance increase ~50–60 km deep that extends from central Costa Rica to Panama. Compared to well-located seismicity, this boundary is offset to the NE from the Cocos plate Benioff zone beneath northern CT, and remains observable through a gap in seismicity farther to the southeast. This offset makes it difficult to interpret this feature as related to the presently subducting lithosphere. Instead, we propose that the 50–60 km deep boundary marks the Moho of a lithospheric fragment left behind under the CT in the course of Panama Triple Junction migration through Costa Rica over the last 10 Ma. Our interpretation accounts for the geophysical, geochemical, structural, and geomorphic observations in the literature explaining the complex geodynamic scenario observed in southern Costa Rica.

Plain Language Summary Subduction of oceanic plates is typically associated with both intense seismic activity and volcanism. A segment of the subduction zone in southern Costa Rica and Panama lacks both of these attributes at present. The area has an unusual tectonic environment that is changing relatively rapidly (on the time scale of 1–3 million years) due to geometry and motion directions of three plates, Cocos, Nazca, and Caribbean, that are joined here forming a triple junction. Alternate scenarios proposed to account for the recent rise of very high mountains, the cessation in volcanism, and the absence of seismicity in the area include subduction gaps, flat subduction, and subducted lithosphere lost just recently (geologically speaking). We develop new seismological constraints on Earth internal layering in the upper 100 km beneath southern Costa Rica. We find an unexpected near-horizontal boundary 50–60 km beneath this region. It is well below the crust mantle boundary of the Caribbean plate, and it is not aligned with well-located seismicity of the currently subducting Cocos plate. We interpret this feature as a fragment of previously subducted oceanic lithosphere stranded due to the rapid rearrangement of plate configuration in Costa Rica-Panama border region.

1. Introduction

The recycling of Earth materials through subduction is the driving force of plate tectonics. The downgoing oceanic lithosphere can be of diverse nature with regimes of over-thickened crust along ridges, seamounts, and transform boundaries that alter composition, thickness, and relief of the plate (Stern, 2002). These features impact the dynamics of the subduction process and have significant influences on the Earth's surface expression (e.g., Morell et al., 2016). A particularly complex tectonic environment can be observed in southern Costa Rica where the nature of subducted materials dramatically changes over a distance of ~500 km from the typical oceanic crust produced at the East Pacific Rise to seamounts and the ~20-km-thick Cocos Ridge derived from the Galapagos Hot Spot track, and the Panama Fracture Zone (PFZ) transform boundary (Figure 1).

The surficial expression of changes in the nature of the downgoing slab can be noticed from northern to southern Costa Rica. Near-orthogonal subduction of typical oceanic lithosphere from the East Pacific Rise

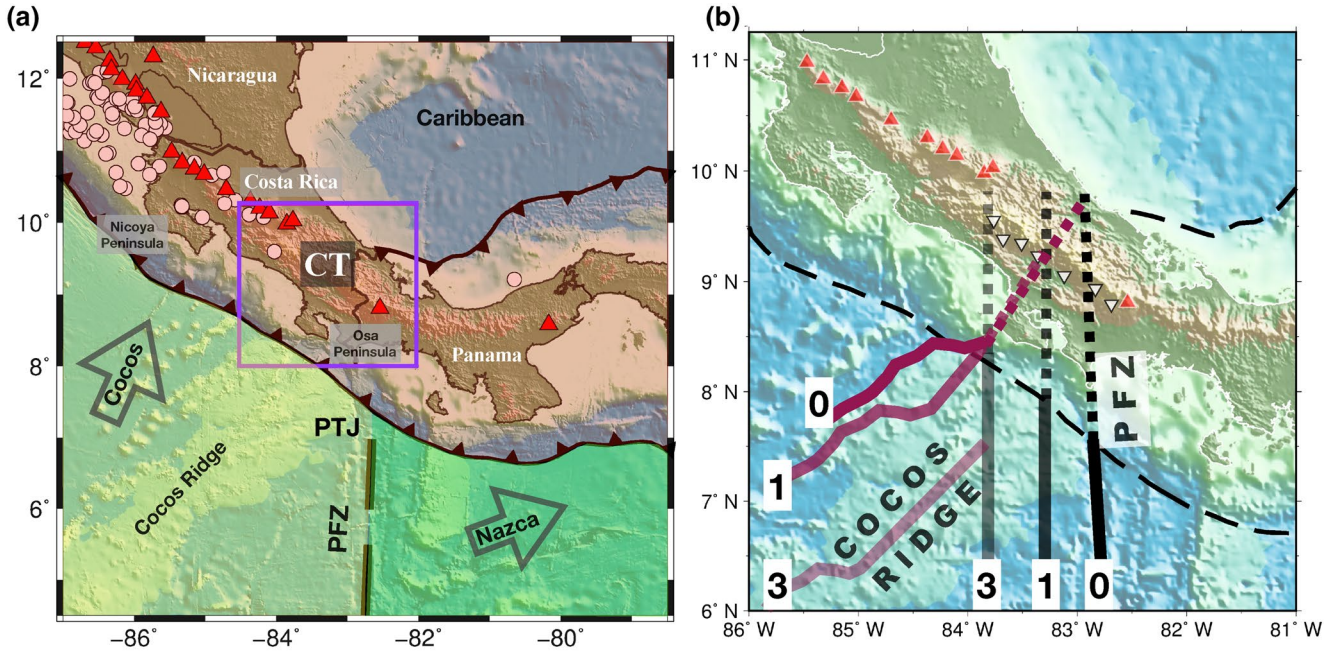

Figure 1. (a) Regional map of plate boundaries, Caribbean plate (shaded red), Cocos plate (shaded yellow), and Nazca plate (shaded green). Red triangles represent active volcanoes, white dots are 4.0+ magnitude earthquakes deeper than 40 km (ISC). Topographic data from GMRT data set (Ryan et al., 2009). PTJ between the Caribbean, Cocos, and Nazca plates. (b) Tectonic reconstruction of southern Costa Rica adapted from Morell (2015). Black line represents the southeastern migration of the PTJ over the last 3 Ma. Burgundy line is approximate position of the northwestern boundary of the Cocos Ridge over the last 3 Ma and numbers mark ages in millions of years. ISC, International seismological center; PFZ, Panama Fracture Zone; CT, Cordillera de Talamanca; PTJ, Panama Triple Junction.

occurs in the north, with subduction signatures of upper-plate volcanism, a clearly defined Wadati-Benioff zone, and a deep offshore trench (Lücke & Arroyo, 2015; Protti et al., 1995). To the south where the Cocos Ridge and PFZ converge with the Costa Rican land mass, the nature of subduction and its typical geochemical signatures change (e.g., Gazel et al., 2019). Arc-typical volcanism is absent and seismicity is reduced, with no magnitude 4.0+ earthquakes deeper than 70 km observed from south Costa Rica to Colombia (Figure 1). The lack of subduction signatures is spatially coincident with the very extreme (3 km) and recent uplift of the Cordillera de Talamanca (CT) (Gräfe et al., 2002; MacMillan et al., 2004; Morell et al., 2019; Zeumann & Hampel, 2017).

Presently, three primary hypotheses have been published to explain the change in the southern Central American subduction zone, all focusing on the geometry and history of the Cocos plate beneath southern Costa Rica. These hypotheses range from a steeply dipping aseismic slab (Dzierma et al., 2011; Lücke & Arroyo, 2015), to a nearly or completely flat slab (Fisher et al., 2004; Gardner et al., 1992; Morell et al., 2016), to a slab window being present (Gazel et al., 2011, 2019; Johnston & Thorkelson, 1997). Each model predicts possible impedance structures and can be directly tested. In a typical subduction zone, we expect to see a Moho associated with the overriding plate, and a deeper Moho for the subducting slab. This is observed in northern Costa Rica by Linkimer et al. (2010); where they introduce a nomenclature that will be followed in this paper: The deeper Moho within the subducting plate is called M1, and the shallower Moho of the overriding plate is called M2. For a flat slab scenario, we expect to see only the M1 boundary with an increase in impedance because the upper plate and subducting plate are coupled and the impedance of the lower crust should be similar to the impedance of the oceanic subducting crust. This boundary should be at a depth corresponding to the combined crustal thickness of both the upper and the subducting plates. If the impedances were not similar or the upper crust and the slab were not coupled, then we should expect to see both the M1 and the M2 boundaries. For the slab window (i.e., plate not reaching the area we study), and the broken slab (i.e., slab detaching and descending), we should expect to see a single relatively shallow boundary M2.

This study seeks to place constraints on the tectonic structure beneath southern Costa Rica. We utilize the receiver function (RF) methodology to detect and characterize impedance boundaries in the crust and the upper mantle beneath the southwestern flank of the CT. We compare our receiver function results to earthquake hypocenter data from the National Seismological Network (RSN) of the University of Costa Rica. Our results show that the pattern of impedance contrasts is consistent with two distinct near-horizontal boundaries underlying the CT. We interpret a boundary at ~20–30 km depth as the Moho of the overriding Caribbean plate, and we associate the boundary at 50–60 km depth with the Moho of an underthrust portion of the lithosphere. Placing these boundaries in the context of regional seismic activity associated with the presently subducting Cocos plate, we propose a scenario that involves a geologically recent break in the continuity of the lithosphere underthrust beneath Central America.

2. Geological Background

The Costa Rican land mass is located on the Caribbean plate overlying the subducting Cocos plate. In southern Costa Rica the migrating PFZ marks a triple junction between the Cocos, Nazca, and Caribbean plates (Figure 1). The Cocos plate subducts obliquely beneath the Caribbean plate with variable rates of convergence between northern (~80 mm/y) and southern (~90 mm/y) Costa Rica (DeMets, 2001; Kobayashi et al., 2014). The overriding Caribbean plate is a part of the Caribbean large igneous province that was likely formed ~94–89 Ma by the hot spot presently beneath the Galapagos Islands (Kerr et al., 1997). In the north, the Cocos plate was formed ~17 Ma ago at the East Pacific Rise (Ranero et al., 2003), whereas the oceanic crust converging with southern Costa Rica formed at the Cocos-Nazca Spreading Center and was overprinted by the Galapagos Hot Spot ~13–14.5 Ma ago (Barckhausen et al., 2001; Werner et al., 1999). The Galapagos Hot Spot influence on the Cocos plate is revealed by bathymetric and seismic studies that describe the presence of seamounts (Barckhausen et al., 2001; Hoernle et al., 2002) and the 20-km-thick, 200-km-wide Cocos Ridge offshore southern Costa Rica (Walther et al., 2003).

The timing of the Cocos Ridge convergence with the Central American landmass is debated, with estimates from 0.5 Ma (Gardner et al., 1992) to 8 Ma (Abratis & Wörner, 2001). More recent estimates from plate motion reconstructions, ocean drilling, and active source seismic imaging converge at 1–3 Ma (MacMillan et al., 2004; Morell et al., 2008, 2012, 2019; Vannucchi et al., 2013). Interestingly, the location of the subducting Cocos Ridge coincides with an interruption of subduction-related volcanism in southern Costa Rica. The exact time of arc volcanism cessation varies in the literature, with more recent studies (e.g., Gazel et al., 2011) favoring a date of ~6.5 million year.

Subduction geometry in Costa Rica is also variable from north to south. In the north, the slab is well imaged and can be observed dipping ~84° to a depth of ~200 km (Protti et al., 1995), in central Costa Rica the dip is ~15° at 25–30 km changing to ~65° at ~125 km depth based upon concentrated seismicity (Husen et al., 2003). In central to southern Costa Rica, the slab is estimated to be steeply dipping on the basis of seismic imaging (Dzierma et al., 2011) and by gravitational modeling coupled with local earthquake locations (Lücke & Arroyo, 2015); however, earthquakes deeper than 70 km are not observed under the CT.

The seismological constraints on the crustal thickness throughout Costa Rica range ~27–42 km in northern Costa Rica (Deshon et al., 2006; Linkimer et al., 2010; MacKenzie et al., 2008; Protti et al., 1996). In central to southern Costa Rica the depth to the upper plate Moho has been imaged by receiver function analysis (Dzierma et al., 2011) to be 30–40 km, whereas tomographic models place it at ~30 km (Dinc et al., 2010), and active source imaging shows it to be 40 km beneath the volcanic front (Hayes et al., 2013).

The tectonic setting of southern Costa Rica has changed dramatically over the past ~10 Ma. Plate reconstructions of the region suggest an incredibly complex plate motion and realignment (Morell, 2015), resulting in significant changes in the upper plate deformation and where the plates subducted. These changes are mostly governed by the development of the Panama Triple Junction (PTJ) between the Cocos, Nazca, and Caribbean plates ~8.5 Ma ago, the introduction and subduction of rougher oceanic crust ~3–4 Ma ago, and the collision of the Cocos Ridge most likely ~1–3 Ma. As the triple junction reached the convergent margin with the Caribbean plate, it migrated southward along the margin (Figure 1b), altering where the Cocos and Nazca plates subducted beneath the Caribbean plate.

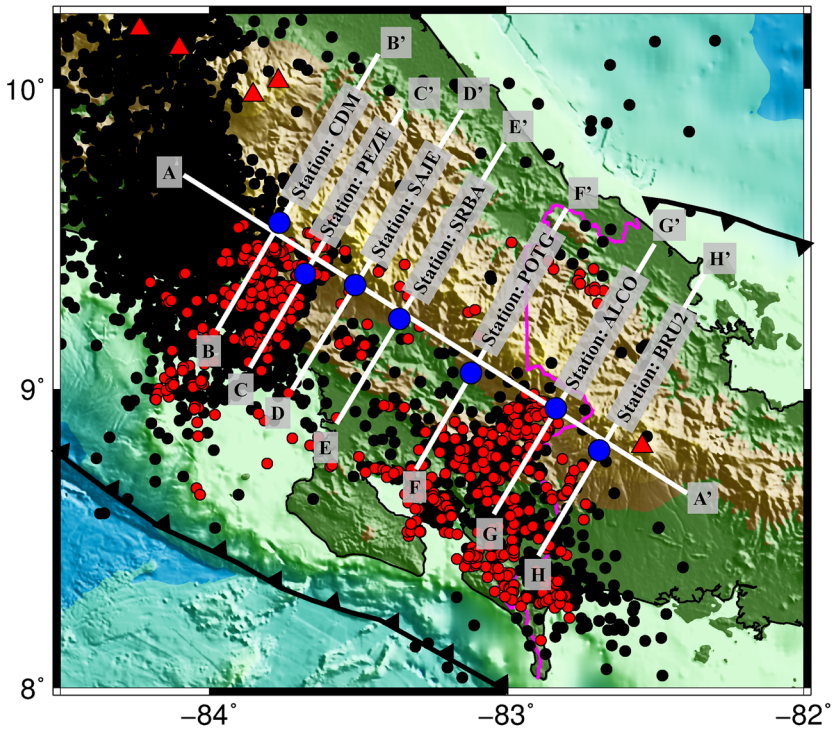

Figure 2. Map of southern Costa Rica. White lines are seismicity transects shown in Figures 4, 5 and 6. Blue circles are seismic stations used in this study, black triangle lines are convergent margins, small red circles are precisely re-located earthquakes (Lücke & Arroyo, 2015), and small black circles are +3.0 magnitude earthquakes between years 2007 and 2019 (Linkimer et al., 2018). Magenta line is the political border between Costa Rica and Panama. Topographic data from GMRT data set (Ryan et al., 2009).

2.1. Data

We use publicly available data from continuously recording seismic instruments along the southwestern flank of the CT (Figure 2) belonging to RSN (TC network), OVSICORI-UNA (OV network), and ChiriNet (PA network). We used data from ~2014 to 2018 for OV network stations CDM, PEZE, SRBA, and POTG, ~2014 to 2020 for ChiriNet station BRU2, and from the end of 2018 through 2020 from recently installed TC network stations ALCO and SAJE. All data are archived at the Incorporated Research Institutions for Seismology (IRIS) data management center. We focused on three component records of the first arriving compressional wave (P) from teleseismic earthquakes, at frequencies of 0.02–1 Hz. We inspected 8790 P, Pdiffracted, and PKP phases from events with magnitudes of 5.5+ at epicentral distances (EPI) of 20°–180°. These records were visually inspected for the presence of coherent earthquake signals, integrity and continuity of records on all three components, and the absence of excessive noise. A total of 1,163 records were selected for analysis, with individual sites having 35–329 records (Table 1).

Seismicity data used in this study are a product of the RSN and were described in detail in Linkimer et al. (2018). Events used in this study occurred between 2007 and 2019. We also include a subset of seismicity that was relocated in the course of computing a slab depth model for Costa Rica (Lücke & Arroyo, 2015).

3. Methods

For this study, we use the receiver function methodology (Ammon, 1991; Langston, 1977, 1979) to image the crust and the upper mantle beneath the stations. When a P wave encounters a change in impedance (velocity × density) across an interface some of the P phase energy is converted into sec-

Table 1
List of Seismic Stations Used in This Study With Relevant Information for Locations, Elevation, Number of Receiver Functions Produced, Number of Raw Earthquake (EQs) Data, and Time/Depth Estimates for the M1 and M2 Pulses

Network	Station	Lat. (°)	Long. (°)	Elevation (m)	No. of EQs	No. of RFs	Beam pulse M1 (s)	Beam pulse M2 (s)	Beam pulse M1 (km)	Beam pulse M2 (km)
OV	CDM	9.55	−83.76	3,494	1,382	329	5.8	3.25	54.9	27.7
OV	PEZE	9.38	−83.68	807	1,373	121	5.3	2.2	50.2	18.7
TC	SAJE	9.34	−83.51	1,351	483	65	6.25	3.4	59.2	28.9
OV	SRBA	9.23	−83.36	974	1,124	226	5.75	N/A	54.5	N/A
OV	POTG	9.05	−83.12	674	1,164	209	6.2	2.7	58.7	23
TC	ALCO	8.93	−82.83	1,504	167	35	6.4	3.7	60.6	31.5
PA	BRU2	8.79	−82.69	1,320	3,097	178	6.4	2.4	60.6	20.4

Abbreviation: RFs, receiver functions.

ondary shear waves (Ps) which are recorded seconds after the initial P wave (Phinney, 1964). These Ps phases originate close to the receiver which allows investigations of the crust and upper mantle beneath the receiver. If the material interface happens to be inclined, the converted Ps phases from different back-azimuths are generated at varying depths which alters the time in which the Ps phases reach the receiver. This change in time results in a systematic directionally dependent P-Ps move-out that is governed by the strike and the dip of the interface (Cassidy, 1992; Levin & Park, 1997; Savage, 1998; Shiomi & Park, 2008). Further interpretation of these phases is based upon the polarity of the pulse after interacting with an impedance boundary. Positive polarity in receiver function time series implies an increase in impedance with depth, whereas negative polarity implies a decrease in impedance (Figure S1). We utilize the Multitaper spectral correlation (MTC) RF technique (Park & Levin, 2000), which makes the use of higher frequency data (e.g., PKP phases) feasible and incorporates frequency domain move-out corrections discussed in Park and Levin (2016). Prior to analysis, we rotate three-component records of teleseismic P waves into the LQT coordinate system, with L aligned along the raypath, Q in the same vertical plane with L, and T orthogonal to it. This coordinate system effectively separates compressional (P) waves (on the L component) from shear (Ps) waves (on Q and T components). Deviations in local Vp or Vs from those chosen to compute the rotation angles may result in some P wave energy remaining, especially at longer periods that sense both the crust and shallow upper mantle. This study focuses on the Q component of Ps waves that reflects changes in impedance with depth.

For each station, we generate RF gathers for events binned by back-azimuth or EPI (Figure 3), and use them to identify likely impedance contrasts beneath southern Costa Rica. We use 10° bins in either back-azimuth or distance, with 50% overlap so an earthquake at backazimuth 145° would be included in both the 140° and 150° bins. Each bin shown has a minimum of two earthquakes. To preserve the amplitudes of the Ps phases, the RFs are normalized in the frequency domain with a factor of $2f_N/f_c$ where the Nyquist frequency $f_N = 1/(2\tau)$, and f_c and τ are the cutoff frequency and the sampling interval, respectively (see Park & Levin, 2000). All records shown are corrected for move-out using compressional velocity (Vp) values of 6.3 km/s and 8.0 km/s in the crust and the mantle, respectively, and Vp/Vs ratio of 1.74, adapted from the local velocity model used to locate earthquakes in Linkimer et al. (2018). After the move-out correction Ps phases formed at horizontal interfaces should arrive at the same time from all directions and all distances.

The majority of earthquake data comes from between 150° – 170° and 260° – 300° back-azimuth from the stations (Figure S2). We construct narrow beams of receiver functions from earthquakes between 150°–170° back-azimuth and 30°–50° degrees of EPI and use the resulting time-series to measure delay time values of peaks we chose for interpretation (Figure 4). By using a narrow beam instead of a stack of the entire data set we hope to avoid pulse shape distortions from local velocity heterogeneity beneath the station. Figure S3

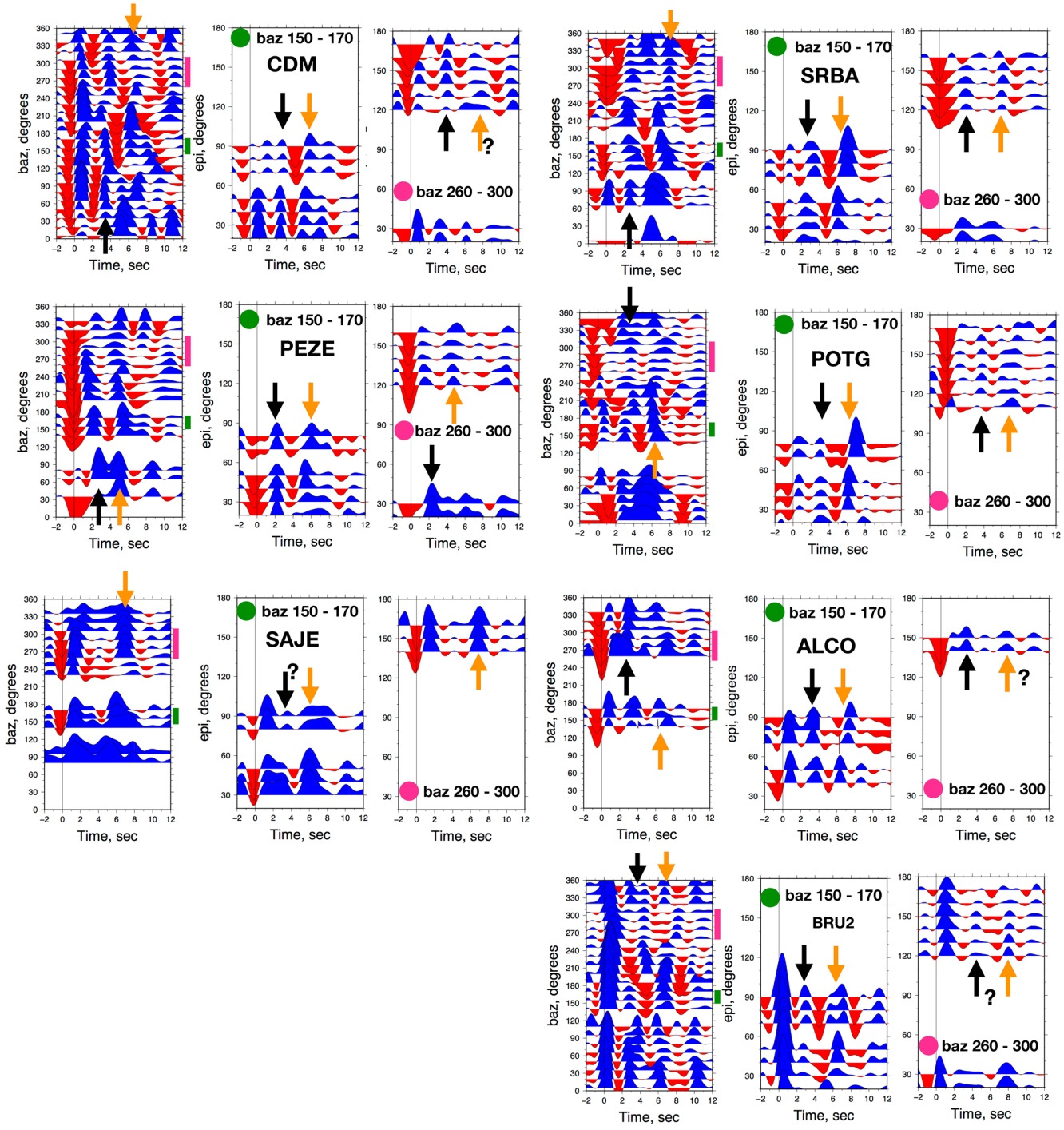

Figure 3. A back-azimuthal and two epicentral receiver function gathers shown for each site. All plots are rotated to LQT coordinates. Epicentral plots are focused on two directions where the majority of the data are concentrated. Plots with green circles are ~150°–170°, and plots with pink circles are ~260° – 300°. Black arrows indicate our interpreted M2 pulse, whereas orange arrows represent the M1 pulse.

shows the pierce points of all rays used to compute RFs; the beam we have chosen samples the foothills of the CT.

The delay time of a Ps phase is used to estimate the depth to the impedance interface (Cassidy, 1992; Gurrola & Bernard Minster, 1998), by using the equation:

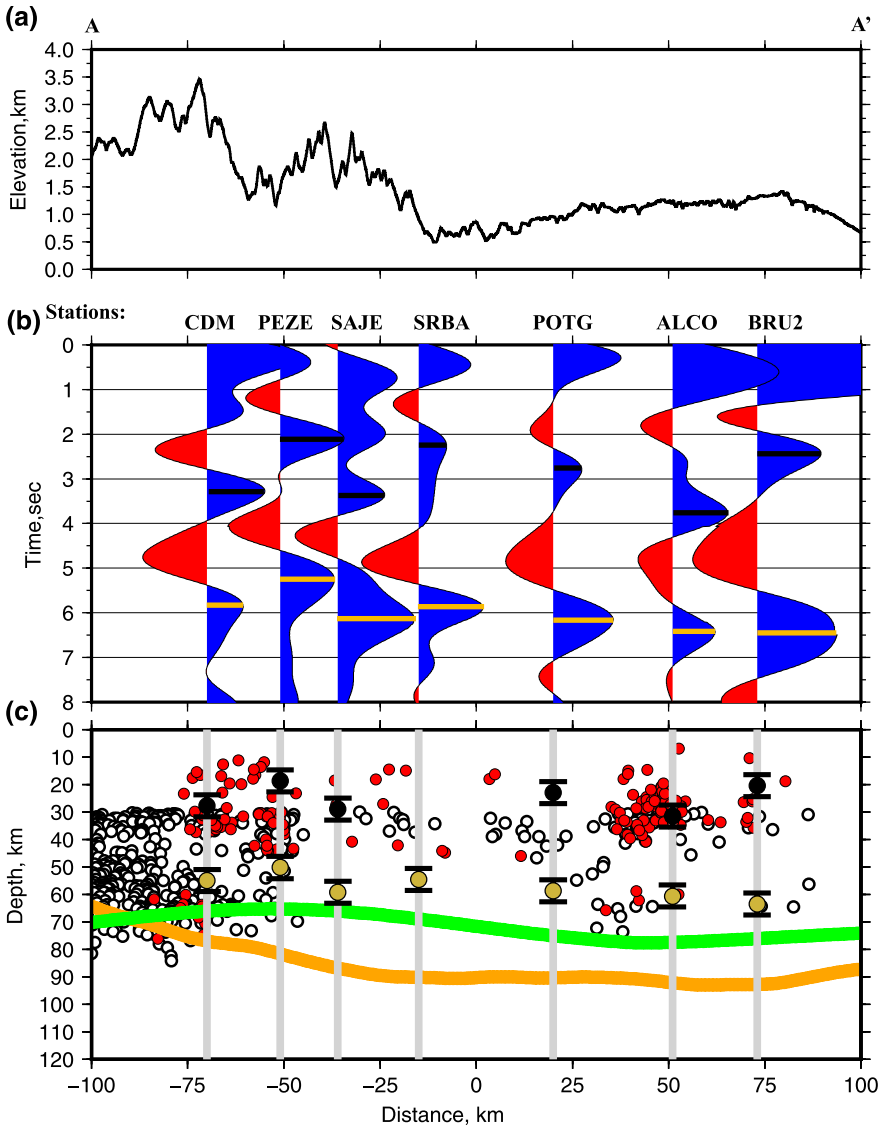

Figure 4. (a) Topography along the A-A' transect from GMRT data base (Ryan et al., 2009). (b) Beam formed receiver functions along the western flank of the Cordillera de Talamanca (see Figure 2 for transect location). Black and gold lines in middle panel show times chosen for computing the depths of boundaries beneath each site. (c) Seismicity along the transect A-A', we use earthquakes 20 km toward the southwest and 5 km to the northeast from the transect and +3.0 magnitude, open circles are events deeper than 30 km from the catalog of Linkimer et al. (2018) and red circles are re-located earthquakes from Lücke and Arroyo (2015). Green and orange lines show traces of the slab surfaces from Slab2 (Hayes, 2018) and Lücke and Arroyo (2015), respectively. Black and gold circles show depths of boundaries. Black lines above and below the black and gold circles are ±4 km uncertainty estimates for our time to depth conversion.

$$h = \frac{t}{\left(\sqrt{\frac{1}{V_S^2} - p^2} - \sqrt{\frac{1}{V_P^2} - p^2}\right)} \tag{1}$$

where t is the delay time of the peak of the phase's amplitude, V_p and V_s are P and S waves velocities, and p is the ray parameter, which can be taken as zero because of the move-out correction. We adopt the 1D P-wave velocity model used by RSN for measuring earthquake locations to estimate depths from our receiver function delay times (Table S1).

Uncertainty of our time to depth conversion is mainly based upon the time we input. The V_p, V_s, and V_p/V_s ratio values also account for uncertainty in our time to depth estimates. We choose to use the 1D velocity model that was used for the earthquake location, as well as for relocation of events in Lücke and Arroyo (2015), and Linkimer et al. (2018) which has a V_p/V_s ratio of 1.74. By altering the V_p/V_s ratio by 5% we produce uncertainties of ±4 km. The timing of the peak of the pulse will change in back-azimuth as the structure of the upper mantle and the crust vary with direction, and by the frequency; increasing frequency will make a "sharper" peak. Due to the broadness of our peaks we estimate ±0.25 s of uncertainty which results in ±2 km in our depth conversion estimates.

A feature of the MTC methodology (Park & Levin, 2000, 2016) is to produce arrivals prior to the 0 time in the receiver function; these reflect the noise level in the data that were combined to form a single binned RF time series. On the other hand, phases seen close to, but after the 0 time, reflect shallow (first kilometers in depth) structure near the receiver. These phases are hidden by the P wave projection in the radial and transverse coordinate frame. Their polarity reflects very shallow structure, which is not a target of this study.

To provide calibration for our methodology, we generated receiver functions for a long-running seismic site, JTS, in northern Costa Rica (Figure S4). This site was investigated in Linkimer et al. (2010) where the authors identified phases from the crust-mantle boundaries within both the overriding and the subducting plates. We observe the same phases with respect to time and back-azimuth, giving confidence that our procedures yield results consistent with previous work.

4. Results

We present our results as groups of RFs plotted by back-azimuth (BAZ) and EPI in Figure 3, and beamformed pulses with a transect of seismicity and topography (Figure 4). Stations SAJE and ALCO lack robust back azimuthal and EPI sweeps primarily due to the limited recording time. Below we provide brief summaries of observations at each site.

4.1. Receiver Functions and Phases Chosen for Interpretation

CDM: Between backazimuths 150°–340° a positive pulse (M1) is present between 6 and 7 s, while between backazimuths 0°–120° positive pulses appear earlier and later (5–7 s, in narrow ranges). SE epicentral gather shows a clear positive phase at 6–7 s. While its move out is not consistent with a purely horizontal interface we do not think this is a multiple due to the absence of a clear "primary" phase at 2–3 s delay. From the NW a broad positive pulse is present between 7 and 8 s delays. Between 3 and 4 s a positive pulse (M2) is present from almost all directions, and is observable in epicentral gathers from the SE and the NW.

PEZE: Pulse (M1) between 5 and 6 s visible from all directions and clearly observed in both epicentral gathers. A clear phase between 2 and 3 s (M2) on the SE epicentral gather and in short-distance RFs from the NW. Backazimuth expression of this phase is less clear. A strong positive-negative phase in the first 1.5–2 s likely interferes with it.

SAJE: The M1 phase is clearly observed in both epicentral gathers, with SE arrivals being earlier (~6 s) than the NW ones (~7 s). Backazimuth gather is incomplete due to short duration of data recording at this site. M2 phase is visible from the most directions samples, except for backazimuths 230°–250°. The M2 phase is not obvious in the backazimuth gather and the NW epicentral gather. A likely candidate for it is a weak pulse between 3 and 4 s on the SE epicentral gathers.

SRBA: The M1 phase at backazimuths 240°–360°, and in the corresponding NW epicentral gather, the clear positive pulse is seen between 7 and 8 s. Between backazimuths 120°–230° a positive pulse arrives between 6 and 7 s. The corresponding SE gather shows two discontinuous positive arrivals in this time window. A broad positive phase between 4 and 7 s in backazimuth range 0°–100° likely combines the M1 and an earlier pulse that reverses its polarity between backazimuths 120°–300°. The M2 pulse between 2 and 3 s is clearly observed from all directions, and in the NW epicentral gather. In the SE epicentral gather it is broadened in RFs from short distances.

POTG: The M1 positive pulse is present between 6 and 7 s delay from almost all directions and in both epicentral gathers. The SE gather shows two discontinuous positive arrivals in this time window. A broad

positive phase between 4 and 7 s in backazimuth range 0°–100° likely combines the M1 and an earlier pulse that reverses its polarity between backazimuths 120° and 180°. A relatively weak M2 positive pulse is seen at ~3 s from NW and E directions (backazimuth range 330° through 0°–180°), while from the SW and W a positive pulse arrives closer to 4 s.

ALCO: Positive converted phases are present at delay times 6–8 s from all directions where observations are available. In the SE gather two discontinuous positive arrivals appear in this time window. The phase is clear in the NW epicentral gather although the range of data is limited. Positive pulses are observed between 3 and 4 s from the SE and at ~3 s from NW.

BRU2: Positive pulses arrive 5–7 s from most directions except for the 250–310 range where a positive phase arrives at ~8 s. The SE epicentral gather shows two positive arrivals between delays 6 and 8 s; these pulse likely merge and yield one broad phase in corresponding RFs on the backazimuth gather. A clear positive arrival is seen at ~3 s from 320° to 0° to 180° backazimuth range and in a SE epicentral gather. A very weak arrival at ~5 s observed in the NW epicentral gather likely represents a different phase that displays a clear polarity reversal at backazimuth 190°.

4.2. Impedance Boundaries and Seismicity Distribution

In Figure 4 we present the main results of our investigation, combining time series of beam-formed RFs with a vertical projection of seismicity along the profile formed by our seismic stations. We also show computed depths of interfaces for key phases we chose to interpret and compare them with published depths to the Cocos plate under the profile. We use the same velocity model to estimate interface depths from Ps phase delays and to locate earthquakes on the basis of P and S wave travel time picks, and thus their relative depths should be reliable.

Our receiver functions yield similar results for all sites along the transect (Figure 4 and Table 1). We observe a prominent positive pulse at ~5.3–8 s, corresponding to depths 50.2–60.6 km beneath the stations. We also see another positive pulse in the interval of delays between 2.2 and 3.4 s, corresponding to depths 18.7–31.5 km. Following the convention of Linkimer et al. (2010), we refer to the positive pulse between ~5.3 and 8 s as M1, and the pulse between 2.2 and 3.4 s as M2. Both phases signify increases in impedance with depth. With the exception of site SRBA that has a poorly developed M2 phase, we observe both pulses from broad ranges of directions at each site. After a move-out correction both phases are visible in EPI gathers (Figure 3) and stacked RFs for a narrow range of directions (Figure 4b). Beamformed RFs in Figure 4 also contain a negative phase at delay time 4–5 s, between M1 and M2. This phase appears to be associated with a relatively narrow range of backazimuths (120°–180°) except at site CDM where it is seen from a broad range of arrival directions.

A change in the pattern of seismicity takes place along the strike of the CT (Figure 4c). Moving from the northwest to the southeast, seismicity decreases abruptly approximately beneath site SAJE (distance −50 km along the profile, Figure 4c). Events deeper than ~70 km are not seen to the southeast, and the number of events overall is smaller than under the northwestern flank of the CT. Shallow seismicity reappears between sites POTG and ALCO (distances 25–50 along the profile, Figure 4c). Viewing the seismicity in the direction of subduction contributes additional complexity to our RF results. A clear Wadati-Benioff zone is observed below the northwestern stations CDM and PEZE (profiles B-B' and C-C' in Figure 5). Beneath stations SAJE and SRBA (profiles D-D' and E-E', respectively), we observe virtually no seismicity. Additionally, on the southeastern portion of the transect at stations POTG, ALCO, and BRU2 (profiles F-F', G-G', and H-H' respectively), seismicity deeper than ~30 km may resemble a Wadati-Benioff zone, but is less clear than northern seismicity beneath stations CDM and PEZE. In map view (Figure 2) this seismicity is localized at the on-land extension of the PFZ. While seismicity changes across the transects of seismic stations, the M1 pulse is visible throughout.

5. Discussion

The results of our RF analysis show the presence of a positive impedance pulse (M2) with a 2–4 s delay time, 19–31 km depth, and a positive impedance pulse (M1) at 5–8 s, 50–60 km depth, along the northwestern flank of the CT. These results are interesting, prior investigations of crustal thickness place the depth of the

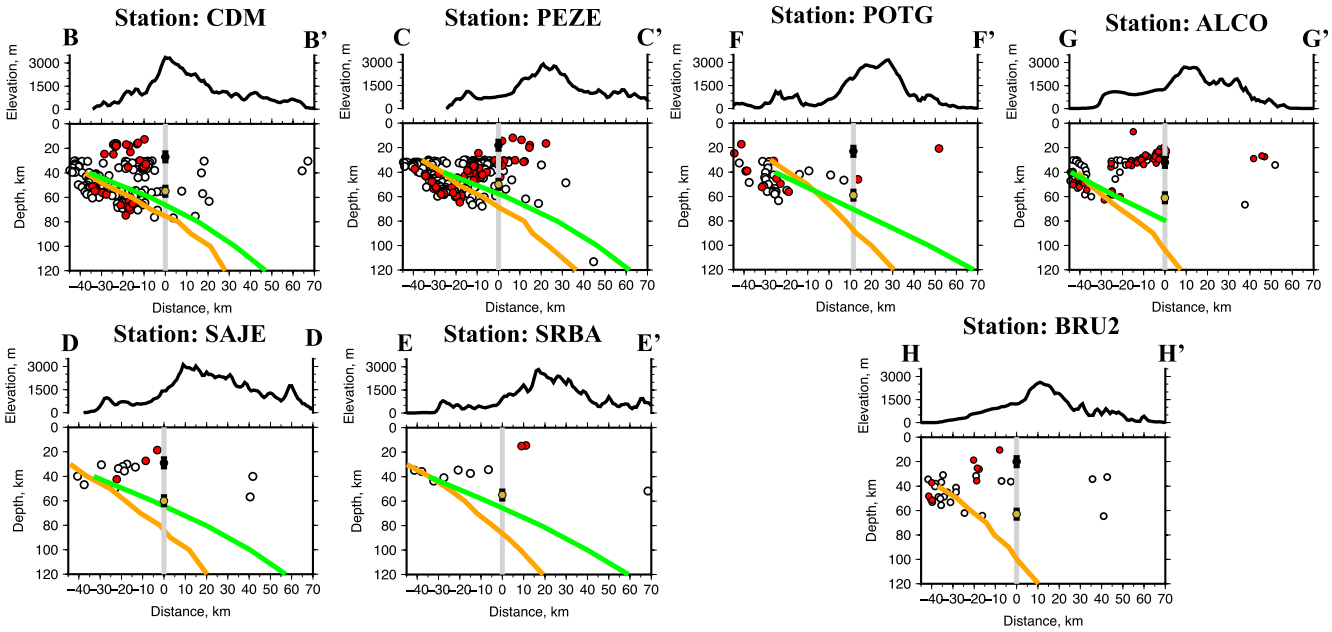

Figure 5. Topographic and seismicity plots along the direction of subduction. Profiles can be observed in map view on Figure 2. The location of seismic sensor (gray line) is marked at 0 km. We use >3.0 magnitude earthquakes (same as in Figure 4) ±5 km from the transect lines. Green line is Slab2 subduction model (Hayes, 2018), orange line is adapted from Lücke and Arroyo. (2015). Black (M2) and gold (M1) circles show depths of impedance boundaries. Black lines above and below the black and gold circles are ±4 km uncertainty measurements for our time to depth conversion.

upper plate Moho between 27 and 33 km in northern Costa Rica, and up to 42 km in the volcanic regions (Linkimer et al., 2010; MacKenzie et al., 2008; Protti et al., 1996). Especially relevant, Dzierma et al. (2011) interpreted the Moho to be at receiver function delay times ∼3.1–3.6 s at sites close to station PEZE. Additional tomographic studies in central Costa Rica also estimate the depth to the Costa Rican upper plate Moho to be ∼30 km (Arroyo et al., 2009; Dinc et al., 2010). Slightly north of our seismic sites a wide-angle refraction and tomography survey estimated the depth of the Moho beneath the volcanic arc to be ∼40 km (Hayes et al., 2013).

Stations CDM, SAJE, and ALCO show M2 phase at 3.25–3.7 s. These stations are likely imaging the Moho of the upper plate at ∼28–31 km. However, the M2 pulse from stations PEZE, POTG, SRBA, and BRU2 is significantly earlier (2.2–2.7 s), corresponding to a boundary that is shallower than in all previous studies, with inferred depths ∼19–23 km. The lack of a prominent Moho signal at these stations could be due to a 10 km thick crust-mantle transition zone imaged by Hayes et al. (2013) within the volcanic arc. This study observed reflections in their shot gathers that they interpreted as likely intrusions, cumulates, relaminated sediment diapirs, and restite. If the impedance contrast within this transition zone is not large enough to produce an observable Ps phase, then it would explain the lack of expected Moho signal at these stations.

Located at depths between 50 and 60 km, the M1 boundary inferred from our data is intriguing. It varies in time throughout the transect but remains present, and can be observed in back-azimuthal and epicentral plots (Figure 3). Additionally, it is well below the expected 30–40 km crust-mantle boundary reported in the previous studies discussed above. Typically, in a subduction zone environment the crust-mantle boundary of the downgoing slab generates a predictable back-azimuthal sinusoidal pattern in delay time based on the relative dip of the subducting oceanic plate. For instance, a steeply subducting slab would be expected to have a more pronounced sinusoid, whereas a gently dipping slab would have a less pronounced sinusoid (Nikulin et al., 2009; Nikulin et al., 2019; Park et al., 2002). Back-azimuthal plots of our receiver functions do not present a pronounced sinusoid in either our pre- or post-moveout corrected receiver functions, implying that we are not observing a steeply dipping impedance boundary.

We do not believe that the M1 pulse is a crustal multiple of the M2 pulse for the following reasons. First, the delay time of the M1 pulse does not fit the expected delay time of a crustal multiple, for instance, at station SRBA the M2 pulse is ∼3 s, the expected multiple would then be found at ∼10 s (Figure S5), whereas the

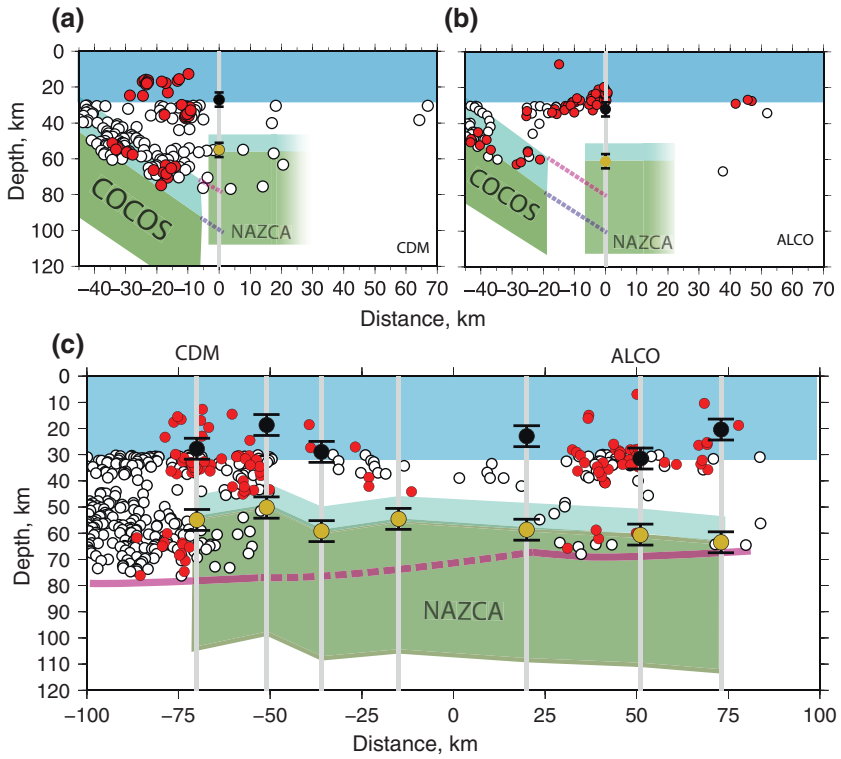

Figure 6. Cartoon illustration of the proposed interpretation for the tectonic structure beneath southern Costa Rica. Red circles are relocated hypocenters from Lücke and Arroyo (2015), white circles are +30 km deep hypocenters from Linkimer et al. (2018), black circles are estimated positions of the M2 pulse, gold circles are estimated positions of the M1 pulse, lines above and below black and gold circles represent an uncertainty estimate of ±4 km. A blue box between 0 and 30 km represents the crust of the upper (Caribbean) plate. Blue boxes represent subducted oceanic crust, shown 20 km thick for the downgoing Cocos plate and 10 km thick for the trapped Nazca plate fragment. Green shapes represent downgoing (Cocos) and trapped (Nazca) lithosphere, shown as being 50–60 km thick on the basis of the likely plate age. Purple lines (solid and dashed) represent the slab top extrapolated from Lücke andArroyo (2015). Dark-blue dashed lines show extrapolated depth of the Cocos plate Moho assuming 20 km thick crust. (a) Interpreted cross section of seismicity beneath station CDM. (b) Cross section of seismicity beneath station ALCO. (c) Same as A-A' cross section of seismicity along the Cordillera de Talamanca.

M1 pulse is found at 5–6 s. Second, it would be unusual for the amplitude of a crustal multiple to be larger than the primary Ps phase, while the majority of the M1 phases are larger than those of M2 phases. Lastly, a crustal multiple from a positive Ps converted phase is required to form a positive-negative doublet. We do not see a coherent negative phase occurring after the M1 pulse in the BAZ or EPI plots.

The nature of seismicity changes drastically from one side of transect A-A' to the other. In the northwest (side A) seismicity is observed occurring down to ~70 km and ceases abruptly for ~75 km along the transect, then reappears near the on-land projection of the PFZ. The lateral similarity of the M1 pulse can be seen across the aseismic region, and interestingly the peak amplitudes of the stations SAJE, SRBA, and POTG are larger than their respective upper plate Moho pulses, M2, at 2.2–3.7 s. Increased amplitudes point to larger impedance contrasts, or in the case of dipping interfaces, a smaller dip (Cassidy, 1992). The lateral position of time and depth of these phases infers that they are likely related to the same geologic feature at depth.

Comparing our results to previous models of the subducting Cocos plate, Figures 4, 5, and 6 show an apparent mismatch between their estimated depth to the slab surface and our results. We place the M1 pulse at ~50–60 km, and interpret it as the Moho of the subducting plate, which should be 5–15 km below the slab top surface, depending on the crustal thickness. This makes it significantly different from the estimated M1 position expected from slab top depths of ~70–80 km proposed by Lücke and Arroyo (2015) and ~60–70 km in the Slab2 model of Hayes et al. (2018).

Uncertainties in the generation of the slab top surfaces could explain a portion of this offset, but not all. For Hayes et al. (2018) model, the stated global average profile has an uncertainty of no more than 10 km. Slab2 provides a smooth slab structure based on the global earthquake catalog, which in turn is built using raytracing in 1D velocity models. In Costa Rica, only earthquakes constrain Slab2 and the reported global uncertainty of 10 km may not reflect bias in absolute space in Costa Rica due to unmodeled slab velocity structure. The Lücke and Arroyo (2015) slab model provides improved spatial resolution relative to Slab2 where earthquakes constrain the top of the slab but uncertainty in their model likely increases away from the events. This study focuses on the CT where there is a clear lack of seismicity and where both Slab2 and Lücke and Arroyo (2015) potentially have increased spatial uncertainty.

The origin of our M1 pulse is thus enigmatic. It is offset, both laterally and vertically, from the re-located seismicity of the subducting Cocos plate (Figures 5 and 6). Dzierma et al. (2010) estimated the isostatic compensation along the CT assuming Airy type isostasy, placing the Moho ∼40–50 km beneath the high peaks of the mountain range. This interpretation however, does not support regional gravitational evidence that places the Moho between 32 and 36 km for the CT (Lücke, 2014; Lücke & Arroyo, 2015). The study conducted by Lücke and Arroyo (2015) focused on two tectonic scenarios to try and match observed gravitational data; the first had a slab steeply subducting to a depth of ∼200 km beneath Costa Rica, and the second had the slab extending to only ∼70 km depth. They report a better fit using the first model, while the second model had an apparent offset. The seismicity clearly terminates at ∼70 km beneath southern Costa Rica making this model difficult to envisage. However, their modeling exercise also suggested that the density of the lower crust beneath the CT had to be smaller than in other parts of Costa Rica.

Comparing our seismicity profiles to the estimated crustal thickness of the Cocos Ridge seems to confirm that the ridge retains its thickness at depth. The Lücke & Arroyo (2015) relocated earthquakes are shown as red circles in Figures 5 and 6, representing a thickness of roughly ∼20 km. This thickness is also reported in studies by Walther et al. (2003) and Sallares et al. (2003), by a wide-angle seismic survey study. This implies that all of the seismicity associated with the subducting slab occurs within the over thickened crust of the Cocos plate. This suggests that the upper portion of the seismicity resembling the slab is likely near the top of the subducting crust.

The M1 feature does not seem to be related to the present-day subduction of the Cocos plate or the Moho of the Costa Rican land mass and thus we explore a different explanation. A plausible interpretation (Figure 6) could be that it represents a segment of formerly subducted lithosphere stranded beneath the CT as a result of the migration of the PFZ and the PTJ over the last 10 million years. In this context it is interesting to note the clear observation of a negative RF phase between M1 and M2 (Figures 3 and 4b). Signifying a decrease in impedance with depth, and positioned 1–1.5 s earlier (thus 8–12 km above), the negative phase preceding the M1 pulse may represent the top of the crust of the stranded fragment of the oceanic lithosphere. Directional dependence (anisotropy) of seismic properties within the crust of the stranded fragment can explain directional variability of the impedance contrast with the overlying Caribbean plate, leading to preferential detection of this feature from a narrow range of backazimuths.

Our preferred scenario is based on a plate tectonic reconstruction of the Cocos-Nazca-Caribbean triple junction by Morell (2015). At and prior to ∼10 Ma ago, only the Cocos plate is subducting beneath southern Central America. This changes ∼8–9 Ma ago when the PTJ reaches offshore northern Costa Rica, and the Nazca plate is actively subducting where the CT is presently. As the PTJ migrated south over the next several million years (see Figure 1b), it is possible that the Cocos plate interaction with the Nazca plate could have produced deformation causing a break or tear of the Nazca plate. Differences in plate motion velocity between the Cocos and Nazca plates could be responsible for this event, where the Cocos is traveling approximately three times faster than the Nazca. If the Cocos plate were able to underthrust part of the Nazca plate as the PTJ moved southeast this could have emplaced a portion of the Nazca crust and lithosphere beneath present-day southern Costa Rica and also caused the cessation of volcanism ∼6.5 Ma (Gazel et al., 2011). The timing of the cessation of volcanism has been argued to be linked to the arrival of the buoyant, younger Cocos Ridge (e.g., De Boer et al., 1995), but studies regarding the beginning of Cocos Ridge subduction place it in a time frame of ∼1–3 Ma (MacMillan et al., 2004; Morell et al., 2008, 2012, 2019; Vannucchi et al., 2013), making it difficult to link Cocos Ridge subduction and the termination of volcanism.

Additionally, studies have credited the Cocos Ridge for the recent uplift of the CT by means of flat slab subduction (Fisher et al., 2004; Morell et al., 2016, 2019). These studies have shown that over the last 1–3 million years the CT have been uplifted ~2–3 km; however, this is problematic when looking at seismological and gravitational models, (Dzierma et al., 2011; Lücke & Arroyo, 2015), which observe a clear steeply subducting slab well below. A possible explanation for these observations is our interpreted lithospheric feature. If prior to or after breaking, the subducting fragment was flatter, this could have been pushed beneath the CT causing the well-documented uplift over the last ~3 Ma. Keeping this feature in place for several million years is harder to explain since it is assumed that basalt within the oceanic crust will convert into eclogite, and the lithospherewill sink into the mantle once subducted, however, some studies report only partial eclogitization at depths of 100–250 km (Abers, 2000); which is well below the feature we detect.

Key arguments against the steep slab hypothesis were the evidence for flat slab subduction (e.g., Fisher et al., 2004; Morell et al., 2019) and the lack of seismicity. Here we show a much larger set of well-relocated seismicity that makes the Wadati-Benioff Zone clearer and also propose a scenario that can reconcile evidence for the alternative shapes of the slab. Potentially, the already subducted part of the Cocos plate is not over thickened and is the force that is pulling the Cocos Ridge down so steeply. Matinod et al. (2013) posited that it would take ~300 km of ridge subduction through the trench before an observed modification in the slab dip would take place. This could potentially mean that the effect from the Cocos Ridge has not yet been seen on the steeply dipping slab. Buoyancy likely plays an important role in keeping the fragment in place. In plate reconstruction models of Morell (2015), note that ~6–8 Ma ago "rough crust" subducting beneath present day southern Costa Rica would have been very young, likely no more than a few million years old based on the reconstructions. If this crust was over thickened and very young and warm, this could account for some buoyancy to keep the fragment in place. Additionally, as described in Antonijevic et al. (2015), if the upper plate and the subducting fragment were coupled, a suction force could also be responsible for holding the fragment in place. Our finding of a subhorizontal positive impedance contrast in the shallow upper mantle beneath a recently uplifted mountain range is similar to the structure reported beneath the Taurus mountains of southern Turkey (Abgarmi et al., 2017). The M2 boundary beneath CT appears more laterally variable as we report point measurements of its depth and do not apply horizontal smoothing inherent in the multistation imaging method used by that study.

The timing of the proposed break in the past Nazca subducting lithosphere can be constrained using the presently observable seismicity and current velocity of the subducting Cocos plate. For instance, the deepest seismicity observed under station CDM is ~70 km and is located roughly 125 km from the trench, this requires the slab to have traversed ~140 km from trench to the present-day seismicity. Using the rate of plate motion of ~90 mm/yr (DeMets et al., 2001), this requires a time of ~1.5 million years, at the minimum, for the Cocos slab to reach the location of the deepest observable seismicity. This estimate is the earliest point where a Nazca break could occur and represents a rough constraint on when the Cocos plate began subducting beneath the present-day CT.

6. Summary

We propose a scenario for the recent oblique tear in the oceanic lithosphere subducting beneath southern Costa Rica. It is developed following Morell (2015) and incorporates new constraints on upper mantle seismic structure we have documented in this paper. The PTJ of Cocos, Nazca and Caribbean plates formed ~8 Ma approximately mid-way between present-day Nicoya and Osa peninsulas (Figure 1a, the latter did not exist yet). To its north the Cocos plate continued "normal subduction," while to its south Nazca plate subducted at a highly oblique angle to the convergent margin, and likely descended at a very shallow angle or was fully flat. The PFZ migrated to the south along the convergent margin and was just north of Osa peninsula by 6 Ma ago. Given the rates of relative plate motion, in the intervening 2 Ma flat Nazca slab likely went all the way beneath the CT, shutting down the volcanism within them. On-land projection of the PFZ migrated through the CT starting at 3 Ma ago and is presently to the SE of the highest elevations in them (Figure 1b). With 80 mm/yr convergence rate most of the CT should be underlain by the material from the Cocos plate, and material from Nazca plate should have descended into the mantle beneath the Caribbean.

Three seismological results suggest that at least a part of it did not, and is instead trapped in the shallow mantle beneath the CT. Our recent study of mantle flow indicators confirmed vigorous flow from the Pacific to the Caribbean directly under the CT (Levin et al., 2020). This finding precludes an existence of a deep-reaching slab there. Our present study identifies a subhorizontal impedance contrast under the CT, most readily explained by a transition from the crust to the mantle lithosphere within a subducted oceanic plate. However, the distribution of local seismicity requires there to be a short subducting slab, especially in the northern part of CT, but does not require it to reach as far as the foothills of the CT where our stations are located.

We propose that recently (between 3 Ma and 1 Ma ago) the lithosphere of the Cocos Plate separated from the already subducted Nazca slab material and began subducting independently. The tear may have initiated due to the increased resistance to subduction when the Cocos Ridge entered the convergent margin ~2.5 Ma ago. Presently the Cocos Plate is going under the stranded Nazca plate fragment in a scissor-like manner. The tear is most likely oblique, with the depth to which Cocos plate material reaches larger in northern CT (under site CDM, Figure 2) than in southern CT (site ALCO). An aseismic region beneath central CT corresponds to the lateral extent of the Cocos Ridge crust that has subducted since 2 Ma ago (per reconstructions in Morell(2015] and Figure 1b). Here the subduction may be nearly flat locally (as envisaged by Antonijevic et al. [2015] in South America), although a short WBZ is seen again where the PFZ projects onto land at present (sites ALCO and BRU2, Figures 3, 5, and 6).

The M1 feature reported in this study as being at ~50–60 km depth beneath the CT is curious. To fully understand this nascent interpretation of a broken Nazca slab remnant beneath the CT more investigation is required to constrain its seismic velocities and character, that is, anisotropy, geometry, and lateral extent. The results of this study point to a more complicated tectonic regime in southern Costa Rica than what has been previously reported, and further develops the mystery as to what is beneath the CT.

Data Availability Statement

Data availability through the archiving services provided by Incorporated Research in Seismology (IRIS) data management system (https://ds.iris.edu/ds/nodes/dmc/). The specific networks that provided data for this study include: Red Sismológica Nacional (https://rsn.ucr.ac.cr/), OVSICORI-UNA (http://www.ovsicori.una.ac.cr/), and ChiriNet (http://redsismicabaru.com/).

Acknowledgments
This research was supported by the US National Science Foundation (NSF) grant OISE 1658648, the University of Costa Rica (UCR) projects 113-B5-704 and 113-B9-911, and by Graduate School – New Brunswick of Rutgers University. Operation of sites ALCO and SAJE would not be possible without the invaluable assistance from RSN engineers L. F. Brenes and J. P. Calvo. Thoughtful and patient reviews from Anonymous and Heather DeShon are gratefully acknowledged. Figures drafted using GeoMapApp and GMT (Wessel et al., 2013).

References

Abers, G. (2000). Hydrated subducted crust at 100–250 km depth. *Earth and Planetary Science Letters*, *176*(3-4), 323–330. https://doi.org/10.1016/s0012-821x(00)00007-8

Abgarmi, B., Delph, J. R., Ozacar, A. A., Beck, S. L., Zandt, G., Sandvol, E., et al. (2017). Structure of the crust and African slab beneath the central Anatolian plateau from receiver functions: New insights on isostatic compensation and slab dynamics. *Geosphere*, *13*(6), 1774–1787. https://doi.org/10.1130/ges01509.1

Abratis, M., & Wörner, G. (2001). Ridge collision, slab-window formation, and the flux of Pacific asthenosphere into the Caribbean realm. *Geology*, *29*(2), 127–130. https://doi.org/10.1130/0091-7613(2001)029%3C0127:rcswfa%3E2.0.co;2

Ammon, C. J. (1991). The isolation of receiver effects from teleseismic P waveforms. *Bulletin of the Seismological Society of America*, *81*, 2504–2510.

Antonijevic, S. K., Wagner, L. S., Kumar, A., Beck, S. L., Long, M. D., Zandt, G., et al. (2015). The role of ridges in the formation and longevity of flat slabs. *Nature*, *524*(7564), 212–215. https://doi.org/10.1038/nature14648

Arroyo I. G., Husen S., Flueh E. R., Gossler J., Kissling E., Alvarado G. E. (2009). Three-dimensional P-wave velocity structure on the shallow part of the Central Costa Rican Pacific margin from local earthquake tomography using off- and onshore networks. *Geophysical Journal International*, *179*(2), 827–849. https://doi.org/10.1111/j.1365-246x.2009.04342.x

Barckhausen, U., Ranero, C. R., von Huene, R., Cande, S. C., & Roeser, H. A. (2001). Revised tectonic boundaries in the Cocos Plate off Costa Rica: Implications for the segmentation of the convergent margin and for plate tectonic models. *Journal of Geophysical Research: Solid Earth*, *106*(B9), 19207–19220. https://doi.org/10.1029/2001jb000238

Cassidy, J. F. (1992). Numerical experiments in broadband receiver function analysis. *Bulletin of the Seismological Society of America*, *82*, 1453–1474.

De Boer, J. Z., Drumond, M., Bordelon, M. J., Defant, M. J., Bellon, H., & Maury, R. C. (1995). Cenozoic magmatic phases of the Costa Rica island arc (Cordillera de Talamanca). In P. Maan (Ed.), *Geologic and tectonic development of the Caribbean plate boundary in southern Central America*. (Vol. 295, pp. 35–36). Boulder, Colorado: Geological Society of America.

DeMets, C. (2001). A new estimate for present-day Cocos-Caribbean Plate motion: Implications for slip along the Central American Volcanic Arc. *Geophysical Research Letters*, *28*(21), 4043–4046. https://doi.org/10.1029/2001gl013518

DeShon, H. R., Schwartz, S. Y., Newman, A. V., González, V., Protti, M., Dorman, L. M., et al. (2006). Seismogenic zone structure beneath the Nicoya Peninsula, Costa Rica, from three-dimensional local earthquake P- and S-wave tomography. *Geophysical Journal International*, *164*(1), 109–124. https://doi.org/10.1111/j.1365-246x.2005.02809.x

Dinc, A. N., Koulakov, I., Thorwart, M., Rabbel, W., Flueh, E. R., Arroyo, I., et al. (2010). Local earthquake tomography of central Costa Rica: transition from seamount to ridge subduction. *Geophysical Journal International*, *183*(1), 286–302. https://doi.org/10.1111/j.1365-246x.2010.04717.x

Dzierma Y., Thorwart M. M., Rabbel W., Flueh E. R., Alvarado G. E., & Mora M. M. (2010). Imaging crustal structure in south central Costa Rica with receiver functions. *Geochemistry, Geophysics, Geosystems*, *11*(8), n/a–n/a. https://doi.org/10.1029/2009gc002936

Dzierma, Y., Rabbel, W., Thorwart, M. M., Flueh, E. R., Mora, M. M., & Alvarado, G. E. (2011). The steeply subducting edge of the Cocos Ridge: Evidence from receiver functions beneath the northern Talamanca Range, south-central Costa Rica. *Geochemistry, Geophysics, Geosystems*, *12*(4). https://doi.org/10.1029/2010gc003477

Fisher, D. M., Gardner, T. W., Sak, P. B., Sanchez, J. D., Murphy, K., & Vannucchi, P. (2004). Active thrusting in the inner forearc of an erosive convergent margin, Pacific coast, Costa Rica. *Tectonics*, *23*(2). https://doi.org/10.1029/2002tc001464

Gardner, T. W., Verdonck, D., Pinter, N. M., Slingerland, R., Furlong, K. P., Bullard, T. F., & Wells, S.G. (1992). Quaternary uplift astride the aseismic Cocos Ridge, Pacific coast, Costa Rica. *Geological Society of America Bulletin*, *104*(2), 219–232. https://doi.org/10.1130/0016-7606(1992)104%3C0219:quatac%3E2.3.co;2

Gazel, E., Hayes, J. L., Ulloa, A., Alfaro, A., Coleman, D. S., & Carr, M. J. (2019). The record of the transition from an oceanic arc to a young continent in the Talamanca Cordillera. *Geochemistry, Geophysics, Geosystems*, *20*(6), 2733–2752. https://doi.org/10.1029/2018gc008128

Gazel, E., Hoernle, K., Carr, M. J., Herzberg, C., Saginor, I., van den Bogaard, P., et al. (2011). Plume-subduction interaction in southern Central America: Mantle upwelling and slab melting. *Lithos*, *121*(1–4), 117–134. https://doi.org/10.1016/j.lithos.2010.10.008

Gräfe, K., Frisch, W., Villa, I. M., & Meschede, M. (2002). Geodynamic evolution of southern Costa Rica related to low-angle subduction of the Cocos Ridge: Constraints from thermochronology. *Tectonophysics*, *348*(4), 187–204. https://doi.org/10.1016/s0040-1951(02)00113-0

Gurrola, H., & Bernard, M. J. (1998). Thickness estimates of the upper-mantle transition zone from bootstrapped velocity spectrum stacks of receiver functions. *Geophysical Journal International*, *133*(1), 31–43. https://doi.org/10.1046/j.1365-246x.1998.1331470.x

Hayes, J. L., Holbrook, W. S., Lizarralde, D., van Avendonk, H. J. A., Bullock, A. D., Mora, M., et al. (2013). Crustal structure across the Costa Rican Volcanic Arc. *Geochemistry, Geophysics, Geosystems*, *14*(4), 1087–1103. https://doi.org/10.1002/ggge.20079

Hayes, G. P., Moore, G. L., Portner, D. E., Hearne, M., Flamme, H., Furtney, M., & Smoczyk, G. M. (2018). Slab2, a comprehensive subduction zone geometry model. *Science*, *362*(6410), 58–61. https://doi.org/10.1126/science.aat4723

Hoernle, K., van den Bogaard, P., Werner, R., Lissinna, B., Hauff, F., Alvarado, G., & Garbe-Schönberg, D. (2002). Missing history (16–71 Ma) of the Galápagos hotspot: Implications for the tectonic and biological evolution of the Americas. *Geology*, *30*(9), 795–798. https://doi.org/10.1130/0091-7613(2002)030%3C0795:mhmotg%3E2.0.co;2

Husen, S., Quintero, R., Kissling, E., & Hacker, B. (2003). Subduction-zone structure and magmatic processes beneath Costa Rica constrained by local earthquake tomography and petrological modelling. *Geophysical Journal International*, *155*(1), 11–32. https://doi.org/10.1046/j.1365-246x.2003.01984.x

Johnston, S. T., & Thorkelson, D. J. (1997). Cocos-Nazca slab window beneath Central America. *Earth and Planetary Science Letters*, *146*(3–4), 465–474. http://doi.org/10.1016/s0012-821x(96)00242-7

Kerr, A. C., Tarney, J., Marriner, G. F., Nivia, A., & Saunders, A. D. (1997). The Caribbean-Colombian Cretaceous igneous province: The internal anatomy of an oceanic plateau. *Geophysical Monograph Series*, *100*, 123–144.

Kobayashi, D., LaFemina, P., Geirsson, H., Chichaco, E., Abrego, A. A., Mora, H., & Camacho, E. (2014). Kinematics of the western Caribbean: Collision of the Cocos Ridge and upper plate deformation. *Geochemistry, Geophysics, Geosystems*, *15*(5), 1671–1683. https://doi.org/10.1002/2014gc005234

Langston, C. A. (1977). The effect of planar dipping structure on source and receiver responses for constant ray parameter. *Bulletin of the Seismological Society of America*, *67*(4), 1029–1050.

Langston, C. A. (1979). Structure under Mount Rainier, Washington, inferred from teleseismic body waves. *Journal of Geophysical Research*, *84*(B9), 4749. https://doi.org/10.1029/jb084ib09p04749

Levin, V., Elkington, S., Bourke, J., Arroyo, I., & Linkimer, L. (2020). Seismic anisotropy in southern Costa Rica confirms upper mantle flow from the Pacific to the Caribbean. *Geology*. https://doi.org/10.1130/g47826.1

Levin, V., & Park, J. (1997). P-SHconversions in a flat-layered medium with anisotropy of arbitrary orientation. *Geophysical Journal International*, *131*(2), 253–266. https://doi.org/10.1111/j.1365-246x.1997.tb01220.x

Linkimer, L., Beck, S. L., Schwartz, S. Y., Zandt, G., & Levin, V. (2010). Nature of crustal terranes and the Moho in northern Costa Rica from receiver function analysis. *Geochemistry, Geophysics, Geosystems*, *11*(1). https://doi.org/10.1029/2009gc002795

Linkimer, L., Arroyo, I. G., Alvarado, G. E., Arroyo, M., & Bakkar, H. (2018). The National Seismological Network of Costa Rica (RSN): An overview and recent developments. *Seismological Research Letters*, *89*(2A), 392–398. https://doi.org/10.1785/0220170166

Lücke, O. H. (2014). Moho structure of Central America based on three-dimensional lithospheric density modelling of satellite-derived gravity data. *International Journal of Earth Sciences*, *103*(7), 1733–1745. https://doi.org/10.1007/s00531-012-0787-y

Lücke, O. H., & Arroyo, I. G. (2015). Density structure and geometry of the Costa Rican subduction zone from 3-D gravity modeling and local earthquake data. *Journal of Geophysical Research: Solid Earth*, *6*(4), 1169–1183. https://doi.org/10.5194/se-6-1169-2015

MacKenzie, L., Abers, G. A., Fischer, K. M., Syracuse, E. M., Protti, J. M., Gonzalez, V., & Strauch, W. (2008). Crustal structure along the southern Central American volcanic front. *Geochemistry, Geophysics, Geosystems*, *9*(8). https://doi.org/10.1029/2008gc001991

MacMillan, I., Gans, P. B., & Alvarado, G. (2004). Middle Miocene to present plate tectonic history of the southern Central American Volcanic Arc. *Tectonophysics*, *392*(1–4), 325–348. https://doi.org/10.1016/j.tecto.2004.04.014

Martinod, J., Guillaume, B., Espurt, N., Faccenna, C., Funiciello, F., & Regard, V. (2013). Effect of aseismic ridge subduction on slab geometry and overriding plate deformation: Insights from analogue modeling. *Tectonophysics*, *588*, 39–55. https://doi.org/10.1016/j.tecto.2012.12.010

Morell, K. D. (2015). Late Miocene to recent plate tectonic history of the southern Central America convergent margin. *Geochemistry, Geophysics, Geosystems*, *16*(10), 3362–3382. https://doi.org/10.1002/2015gc005971

Morell, K. D. (2016). Seamount, ridge, and transform subduction in southern Central America. *Tectonics*, *35*(2), 357–385. https://doi.org/10.1002/2015tc003950

Morell, K. D., Kirby, E., Fisher, D. M., & van Soest, M. (2012). Geomorphic and exhumational response of the Central American Volcanic Arc to Cocos Ridge subduction. *Journal of Geophysical Research: Solid Earth*, *117*(B4). https://doi.org/10.1029/2011jb008969

Morell, K. D., Fisher, D. M., & Gardner, T. W. (2008). Inner forearc response to subduction of the Panama Fracture Zone, southern Central America. *Earth and Planetary Science Letters*, *265*(1–2), 82–95. https://doi.org/10.1016/j.epsl.2007.09.039

Morell, K. D., Fisher, D. M., & Bangs, N. (2019). Plio-Quaternary outer forearc deformation and mass balance of the southern Costa Rica convergent margin. *Journal of Geophysical Research: Solid Earth*, *124*(9), 9795–9815. https://doi.org/10.1029/2019jb017986

Nikulin, A., Levin, V., & Park, J. (2009). Receiver function study of the Cascadia megathrust: Evidence for localized serpentinization. *Geochemistry, Geophysics, Geosystems*, *10*(7). https://doi.org/10.1029/2009gc002376

Nikulin, A., Bourke, J. R., Domino, J. R., & Park, J. (2019). Tracing geophysical indicators of fluid-induced serpentinization in the Pampean flat slab of Central Chile. *Geochemistry, Geophysics, Geosystems*, *20*(9), 4408–4425. https://doi.org/10.1029/2019gc008491

Park, J., & Levin, V. (2000). Receiver functions from multiple-taper spectral correlation estimates. *Bulletin of the Seismological Society of America*, *90*(6), 1507–1520. https://doi.org/10.1785/0119990122

Park, J., & Levin, V. (2002). Seismic anisotropy: Tracing plate dynamics in the mantle. *Science*, *296*(5567), 485–489. https://doi.org/10.1126/science.1067319

Park, J., & Levin, V. (2016). Statistics and frequency-domain move-out for multiple-taper receiver functions. *Geophysical Journal International*, *207*(1), 512–527. https://doi.org/10.1093/gji/ggw291

Phinney, R. A. (1964). Structure of the Earth's crust from spectral behavior of long-period body waves. *Journal of Geophysical Research*, *69*(14), 2997–3017. https://doi.org/10.1029/jz069i014p02997

Protti, M., & Guendel, F. (1995). Correlation between the age of the subducting Cocos plate and the geometry of the Wadati-Benioff zone under Nicaragua and Costa Rica. *Special Papers - Geological Society of America*, 295, 309.

Protti, M., Schwartz, S., & Zandt, G. (1996). Simultaneous inversion for earthquake location and velocity structure beneath central Costa Rica. *Bulletin of Seismological Society of America*, *86*(1a), 19–31.

Ranero, C. R., Phipps Morgan, J., McIntosh, K., & Reichert, C. (2003). Bending-related faulting and mantle serpentinization at the Middle America trench. *Nature*, *425*(6956). 367–373. https://doi.org/10.1038/nature01961

Ryan, W. B. F., Carbotte, S. M., Coplan, J. O., O'Hara, S., Melkonian, A., Arko, R., et al. (2009). Global multi-resolution topography synthesis. *Geochemistry, Geophysics, Geosystems*, *10*(3). https://doi.org/10.1029/2008gc002332

Sallarès, V. (2003). Seismic structure of Cocos and Malpelo Volcanic Ridges and implications for hot spot-ridge interaction. *Journal of Geophysical Research*, *108*(B12). https://doi.org/10.1029/2003jb002431

Savage, M. K. (1998). Lower crustal anisotropy or dipping boundaries? Effects on receiver functions and a case study in New Zealand. *Journal of Geophysical Research: Solid Earth*, *103*(B7), 15069–15087. https://doi.org/10.1029/98jb00795

Shiomi, K., & Park, J. (2008). Structural features of the subducting slab beneath the Kii Peninsula, central Japan: Seismic evidence of slab segmentation, dehydration, and anisotropy. *Journal of Geophysical Research*, *113*(B10), https://doi.org/10.1029/2007jb005535

Stern, R. J. (2002). Subduction zones. *Reviews of Geophysics*, *40*(4), https://doi.org/10.1029/2001rg000108

Vannucchi, P., Sak, P. B., Morgan, J. P., Ohkushi, K., & Ujiie, K., (2013). Rapid pulses of uplift, subsidence, and subduction erosion offshore Central America: Implications for building the rock record of convergent margins. *Geology*, *41*(9), 995–998. https://doi.org/10.1130/g34355.1

Walther, C. H. E. (2003). The crustal structure of the Cocos ridge off Costa Rica. *Journal of Geophysical Research: Solid Earth*, *108*(B3), https://doi.org/10.1029/2001jb000888

Werner, R., Hoernle, K., van den Bogaard, P., Ranero, C., von Huene, R., & Korich, D. (1999). Drowned 14-my-old Galápagos archipelago off the coast of Costa Rica: Implications for tectonic and evolutionary models. *Geology*, *27*(6), 499–502. http://doi.org/10.1130/0091-7613(1999).27%3C0499:dmyogp%3D2.3.co;2

Wessel, P., Smith, W. H. F., Scharroo, R., Luis, J., & Wobbe, F. (2013). Generic mapping tools: Improved version released. *Eos, Transactions American Geophysical Union*, *94*(45), 409–410. https://doi.org/10.1002/2013eo450001

Zeumann, S., & Hampel, A. (2017). Impact of Cocos Ridge (Central America) subduction on the forearc drainage system. *Geology*, *45*(10), 907–910. https://doi.org/10.1130/g39251.1